Journal of Alloys and Compounds 509 (2011) 909–915

Contents lists available at ScienceDirect

Journal of Alloys and Compounds

journal homepage: www.elsevier.com/locate/jallcom

Solution processing of V_2O_5–WO_3 composite films for enhanced Li-ion intercalation properties

Chuan Cai, Dongsheng Guan, Ying Wang*

Department of Mechanical Engineering, Louisiana State University, Baton Rouge, LA 70803, USA

ARTICLE INFO

Article history:
Received 6 July 2010
Received in revised form
19 September 2010
Accepted 22 September 2010
Available online 29 September 2010

Keywords:
Composite materials
Energy storage materials
Scanning electron microscopy
X-ray diffraction

ABSTRACT

We have employed a simple and novel solution processing method to prepare V_2O_5–WO_3 composite films which demonstrate enhanced Li-ion intercalation properties for applications in lithium-ion batteries or electrochromic displays. This solution processing method employs precursors that only contain the elements of V, W, O and H, which avoids impurity elements such as Na that has been commonly used in other solution methods (e.g. using precursors of sodium metavanadate and sodium tungstate solution). The V_2O_5–WO_3 composite films show enhanced Li-ion intercalation properties compared to pure V_2O_5 and WO_3 films. For example, at a high current density of 1.33 A/g, V_2O_5–WO_3 film with a V_2O_5/WO_3 molar ratio of 10/1 exhibits the highest capacities of 200 mA h/g at the first cycle and 132 mA h/g after 50 cycles, while pure V_2O_5 film delivers discharge capacities of 108 mA h/g at the first cycle and 122 mA h/g after 50 cycles. The enhanced Li-ion intercalation properties of the composite films are ascribed to the reduced crystallinity, the increased porosity and thus the enhanced surface area. Both the cyclic voltammogram and chronopotentiometric curves of the V_2O_5–WO_3 film with a molar ratio of 10:1 are distinctively different from those of pure oxide films, suggesting a different Li-ion intercalation process in the V_2O_5–WO_3 film with the molar ratio of 10:1.

1. Introduction

Intercalation compounds as a special family of materials have attracted tremendous research interests recently. The intercalation refers to the reversible intercalation of mobile guest species (atoms, molecules, or ions) into a crystalline host lattice that contains an interconnected system of an empty lattice site of appropriate size, while the structural integrity of the host lattice is formally conserved. Various host lattices are metal dichalcogenides, metal oxyhalides, metal phosphorus trisulfides, metal oxides, metal phosphates, hydrogen phosphates, phosphonates, graphite and layered clay minerals. Guest materials include metal ions, organic molecules, and organometallic molecules. In particular, Li-ion intercalation compounds have received extensive attention due to their applications as electrode materials in Li-ion rechargeable batteries [1–7], electrochemical supercapacitors [8,9], and electrochromic devices [10–12]. Among various transition metal oxides that are capable of intercalating Li ions, vanadium pentoxide (V_2O_5) has been studied widely for several decades [13–17]. V_2O_5 can intercalate Li ions or other molecules due to its layered structure and has a theoretical capacity of 144 mA h/g for one mole Li-ion intercalation per mole V_2O_5 [18,19]. The chemical energy is transformed to electric energy during intercalation and this process can be carried out reversely during deintercalation [20]. Based on this electrochemical property, V_2O_5 has become a promising electrode material for rechargeable Li-ion batteries [21,22], electrochemical supercapacitors [8,9], and electrochromic displays [10,23,24]. However, the Li-ion diffusion coefficient (10^{-12} cm^2/s) and the electronic conductivity (10^{-2}–10^{-3} S/cm) in crystalline V_2O_5 are inherently too low to sustain a large specific capacity at high charge/discharge rates [25–27]. Many studies have been conducted to improve Li-ion diffusion and electronic conduction in V_2O_5 by synthesizing the oxide with a more open crystal structure [28–30] or by incorporating highly conductive materials into V_2O_5 [31–33]. Recently Pan et al. reported that the charge transport in V_2O_5 is improved by forming coherent hydrous vanadium pentoxide–carbon cryogel nanocomposites and the carbon network provides good electrical conductivity, hence the lithium interaction capacity of V_2O_5 is significantly enhanced [17].

Another approach to improve lithium interaction capacity of V_2O_5 is modifying its crystallinity by annealing V_2O_5 xerogel films at 300 °C in nitrogen and air [16] or by adding other electrochemically active species such as titanium dioxide (TiO_2) [34]. In this study, we will incorporate tungsten trioxide (WO_3) into V_2O_5 via solution processing of V_2O_5–WO_3 composite films. WO_3 shows electrochromic properties due to its capability of intercalating various cations (H^+, Li^+, and K^+) and can deliver a capacity of 115 mA h/g theoretically for one mole Li-ion interca-

* Corresponding author. Tel.: +1 225 578 8577; fax: +1 225 578 5924.
E-mail address: ywang@me.lsu.edu (Y. Wang).

0925-8388/$ – see front matter © 2010 Elsevier B.V. All rights reserved.
doi:10.1016/j.jallcom.2010.09.129

lation per mole WO_3. Thus WO_3 has found wide applications in electrochromic displays and smart windows [11,12,35–38]. For example, Wang et al. recently reported the synthesis of uniform crystalline WO_3 nanorods by using a facile hydrothermal process; the assembly of these nanorods without any surfactants results in transparent WO_3 nanorod film, which demonstrates excellent electrochromic properties with high stability over 1000 Li-ion intercalation/deintercalation processes [37]. The electrochromic performance of WO_3 can be further improved by forming V_2O_5–WO_3 composite materials [39]. It has been reported that the composite film with a V_2O_5/WO_3 molar ratio of 0.035:0.965 shows more neutral color and higher coloration efficiency in comparison to pure WO_3 [39]. The WO_3–V_2O_5 composite also exhibits improved catalytic activity, which facilitates its applications for ethanol partial oxidation [40] and NO decomposition [41]. Ranjbar et al. has found that the V_2O_5–WO_3 composite film with a V_2O_5/WO_3 molar ratio of 0.09:0.91 shows better response to hydrogen gas exposure for deeper and faster coloring [42].

V_2O_5–WO_3 composite films have been prepared by pulse laser deposition [43,42] and sol–gel routes [44,39–41]. The sol–gel processing methods offer facile control of the stoichiometry and structure of the films which will affect the charge/discharge capacity and reversibility of the V_2O_5–WO_3 composite films [39]. However, several limitations are also found in the sol–gel routes reported previously. For example, some sol–gel processing methods employ precursors such as sodium tungstate dehydrate (Na_2WO_4), sodium tungstate ($NaWO_3$), sodium metavanadate ($NaVO_3$) [40,44], vanadium oxyisopropoxide, and tungsten hexachloride [41]. Impurity elements such as Na^+ or Cl^- are introduced into the synthetic procedure. Ozer and Lampert have employed a sol–gel method using vanadium triisopropoxide oxide ($VO(OC_3H_7)_3$) and metallic tungsten as the precursors of V_2O_5 and WO_3, respectively. This method avoids those impurity elements; however, the mixed sol obtained by Ozer and Lampert can only remain stable for several days [39]. Most V_2O_5–WO_3 composite films reported in literature have been studied for enhanced catalytic activity or electrochromic performances. In such composite films, WO_3 is usually the major constituent and its catalytic or electrochromic properties are improved by the V_2O_5 addition. There are few reports on the electrochemical properties of V_2O_5–WO_3 composite films for applications in Li-ion batteries.

In this paper, we investigate the Li-ion intercalation properties of V_2O_5–WO_3 composite films for applications as cathode materials in Li-ion rechargeable batteries. We have utilized a simple and novel solution processing method to prepare the V_2O_5–WO_3 composite films with different molar ratios of V_2O_5 and WO_3. This solution processing method employs precursors that only contain the elements of V, W, O and H, and thus avoids to introduce impurity elements such as Na into the sol as other sol–gel methods reported in literature. The resulted solution is stable and remains clear for several months. This solution-processing method also offers simple and precise control of V_2O_5/WO_3 compositions. It is found that V_2O_5–WO_3 composite films deliver higher Li-ion intercalation capacities than both pure V_2O_5 and WO_3 films, due to morphological and structural changes of one oxide caused by the other. In this systematic study, V_2O_5/WO_3 molar ratios are optimized to achieve the highest Li-ion intercalation capacity in the composite film. Furthermore, we have examined the effect of chemical composition, crystallinity, and microstructure of V_2O_5–WO_3 films on their intercalation properties.

2. Experimental

2.1. Preparation of samples

Mixed solutions with different molar ratios of V_2O_5:WO_3 (1:0, 10:1, 4:1, 1:1, 1:4 and 0:1) were synthesized by combining an aqueous vanadium pentoxide sol with a solution of tungsten oxygen ionic species. The vanadium pentoxide sol was prepared using a method reported by Fontenot et al. [45]. 0.136 g V_2O_5 powders (99.6%, Alfa Aesar) was dissolved in 2 ml deionized H_2O and 0.603 ml H_2O_2 (30%, Mallinckrodt) solution. The suspension was stirred until the V_2O_5 powders totally dissolved, resulting in a clear and dark red solution. The solution was then sonicated to get a red brown gel which was dispersed into water in a molar concentration of 0.005 M, and was stirred until it was clear. The tungsten based solution was prepared using a method reported by Yebka et al. [46]. The peroxopolytungstic acid was prepared by dissolving 1.247 g H_2WO_4 (tungstic acid, Alfa Aesar) in 50 ml H_2O_2 (30 wt% in water), resulting in a cloudy white dispersion. The dispersion was stirred for 24 h at 60 °C until a clear colorless solution was obtained. This solution was further diluted in water to reach a molar concentration of 0.005 M. Without further adjusting the pH values (V_2O_5: 2.67 and WO_3: 2.30) of the individual sol and solution, the appropriate amounts of vanadium based sol and tungsten based solution were admixed by stirring for 10 min, giving a yellow solution. A droplet of the sol or solution was drop cast onto a ITO (tin-doped indium oxide) glass (1 in. × 1 in.) and dried under ambient conditions. The masses of all the films were kept at 6×10^{-5} g. The films were then heated at 110 °C for 8 h, followed by heating at 200 °C for 1 h and at 470 °C for 1 h with the same heating rate of 2 °C/min in air. Annealing of the films at 470 °C results in crystalline phases of V_2O_5 and WO_3. Another annealing process was heating the films at 250 °C with a heating rate of 2 °C/min. The effect from amorphous WO_3 on the crystallinity of the composite films can be studied at this temperature.

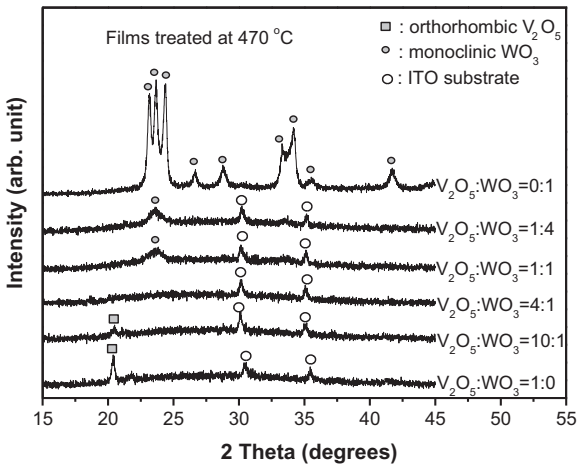

Fig. 1. X-ray diffraction patterns of V_2O_5–WO_3 composite films after annealing at 470 °C in air for 1 h.

2.2. Sample characterizations

The crystalline phases of the films with various V_2O_5/WO_3 molar ratios were analyzed by X-ray diffraction (XRD) using a Rigaku MiniFlex diffractometer with CuKα radiation operated at 30 kV and 15 mA. Scanning electron microscopy (SEM, Quantum 3D FEG) was used to examine the morphology of the pure V_2O_5 and WO_3 films and their composite films with V_2O_5:WO_3 = 4:1 and 10:1 after heat treatment at 470 °C for 1 h. A three-electrode cell was used to investigate the electrochemical properties of the composite films with different molar ratios. A platinum mesh was used as counter electrode and a silver wire in a 0.1 mol/L $AgNO_3$ ethanol solution serves as reference electrode; the Ag/Ag^+ reference electrode has been used for electrochemical measurements including electrochemical characterizations of vanadium-oxide-based electrode materials [17,47,48]. The electrolyte was a 1 mol/L solution of lithium perchlorate (99%, Alfa Aesar) in propylene carbonate (99%, Aldrich). Cyclic voltammetric (CV) measurements were carried out between the potential limits of −1.6 and 0.4 V vs. Ag/Ag^+ using a potentiostat/galvanostat (Model 605C, CH Instrument). The CV curves were recorded after two cycles at a scan rate of 0.05 V/s. The chronopotentiometric measurements were carried out under various current densities.

3. Results and discussion

Fig. 1 shows the X-ray diffraction spectra of the V_2O_5, WO_3, and V_2O_5–WO_3 composite films on ITO substrates annealed at 470 °C for 1 h. The sol–gel-derived V_2O_5 film demonstrates a strong preferential orientation along [0 0 1] direction, which is in good agreement with the previous report [49]. The film derived from the tungsten based solution exhibits a monoclinic phase, as evidenced by the typical peak (0 2 0) at $2\theta = 23.67°$. The monoclinic phase of WO_3 is also observed when the V_2O_5/WO_3 molar ratios are

0:1, 1:4 and 1:1, but its corresponding XRD peaks become weaker as more V_2O_5 emerges in the composite films. The XRD peaks of WO_3 eventually disappear with further increase in V_2O_5 and the orthorhombic phase of V_2O_5 appears when the V_2O_5/WO_3 ratio reaches 10:1. The decease of intensities of diffraction peaks indicates the deterioration of the crystallinity of oxides. As there are no new diffraction peaks other than orthorhombic V_2O_5 and monoclinic WO_3, it can be concluded that there is no second phase. In addition, all the samples are prepared using water-based sol–gel or solution processing methods, as detailed in Section 2; solvents (H_2O and H_2O_2) evaporate and disappear during drying and sintering, and there is no precursor loss. Thus the deterioration of the crystallinity of V_2O_5 and WO_3 is ascribed to the presence of the other oxide. It should be noted that the diffraction peaks of both WO_3 and V_2O_5 disappear when the V_2O_5/WO_3 molar ratio is 4:1, indicating possible amorphization of both oxides.

Fig. 2 shows the XRD patterns of pure oxide and composite films treated at 250 °C for 5 h. Annealing at such a relatively low temperature leads to hydrated films which can be amorphous or nanocrystalline showing broad XRD diffraction peaks. In the XRD patterns of pure tungsten oxide film and composite films with V_2O_5/WO_3 molar ratios of 4:1 and 10:1, no peaks related to WO_3 exist, suggesting tungsten oxide is not crystallized yet at 250 °C. In the XRD pattern of pure vanadium pentoxide film, the peak at $2\theta = 7.82°$ corresponds to the (0 0 1) diffraction of $V_2O_5{\cdot}nH_2O$ and the peak at $2\theta = 20.07°$ is ascribed to orthorhombic V_2O_5, indicating that the film annealed at 250 °C contains a mixture of hydrated films and anhydrous orthorhombic phase; both peaks disappear when WO_3 is added in the composite films with V_2O_5/WO_3 ratios of 4:1 and 10:1. These results suggest that the crystallization process in the composite films is hindered with the coexistence of vanadium and tungsten ions, which occurs even at relatively low temperatures when the oxides are not fully crystallized yet.

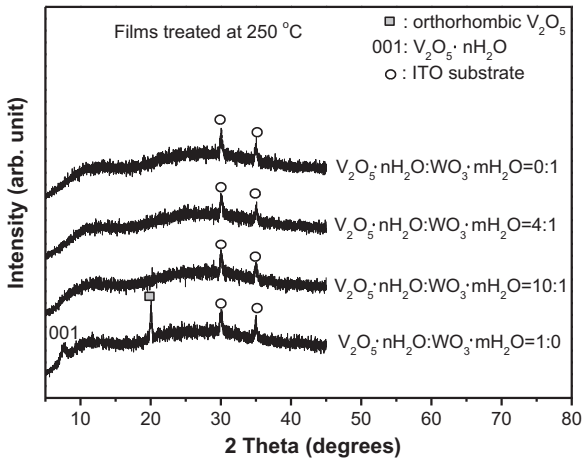

Fig. 2. X-ray diffraction patterns of $V_2O_5{\cdot}nH_2O$–$WO_3{\cdot}mH_2O$ composite films obtained via annealing at 250 °C in air for 5 h.

Fig. 3 shows the top-view SEM images of V_2O_5, WO_3, and V_2O_5–WO_3 composite films with V_2O_5/WO_3 molar ratios of 4:1 and 10:1. The V_2O_5 film is composed of platelet grains and appears dense, as shown in Fig. 3(a). On the other hand, the WO_3 film shows a porous structure as shown in Fig. 3(d), which is different from WO_3 films consisting of nano-sized platelets or needle-like

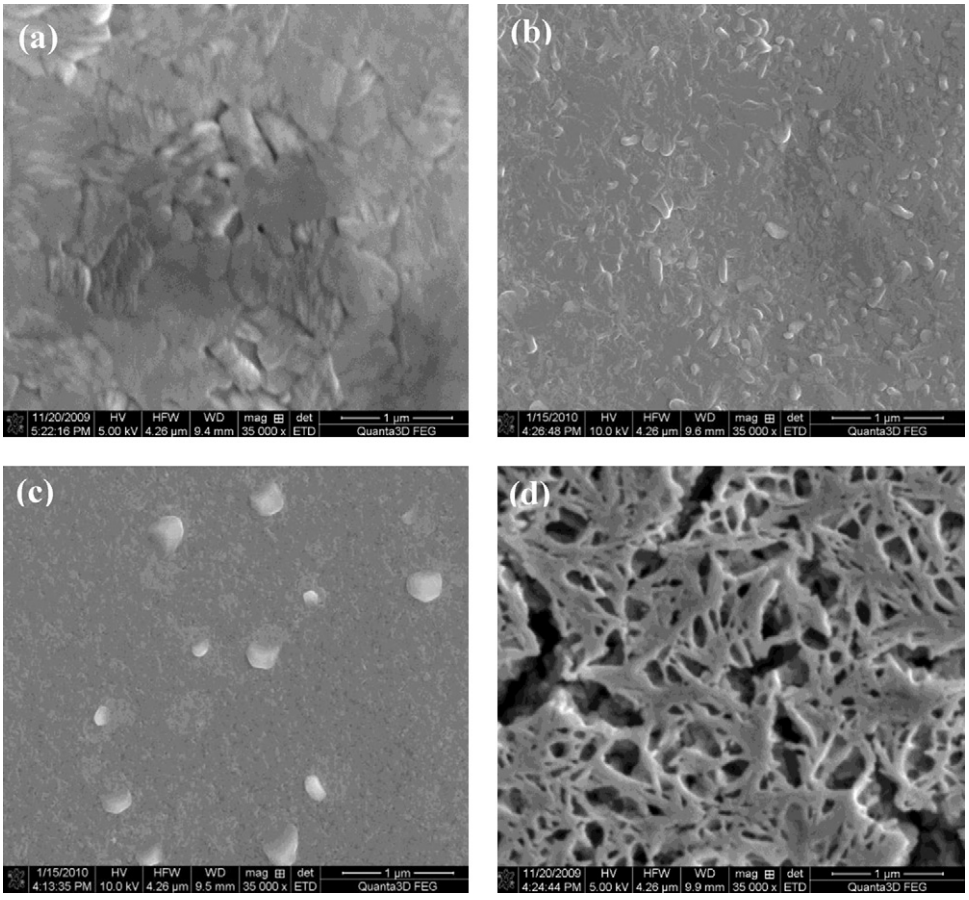

Fig. 3. SEM micrographs showing surface morphologies of (a) pure V_2O_5 film, composite V_2O_5–WO_3 films with V_2O_5:WO_3 molar ratios of (b) 10:1 and (c) 4:1 and (d) pure WO_3 film. All the films are obtained via annealing at 470 °C for 1 h.

textured grains prepared by other solution methods reported in literature [50,51]. Fig. 3(b) and (c) presents the surface morphology of composite films with V_2O_5/WO_3 ratios of 10:1 and 4:1, respectively. It is clear that grain sizes in these composite films are smaller than those in pure V_2O_5 films, indicating the deterioration of crystallinity. There is a small quantity of thick (diameter: ~320 nm) and thin (diameter: ~140 nm) fibers in the composite film with a V_2O_5/WO_3 molar ratio of 4:1. In the case of composite film with a V_2O_5/WO_3 molar ratio of 10:1, many nanofibers with a smaller diameter of about 70 nm exist in the film, as shown in Fig. 3(b).

The cross-section SEM images of films with V_2O_5/WO_3 molar ratios of 1:0, 0:1, and 10:1 are presented in Fig. 4. The cross section of pure V_2O_5 film exhibits a smooth and dense structure, with a thickness of ~215 nm. On the other hand, the cross section of WO_3 film (same mass as V_2O_5 film) shows a rough and porous granular structure and the film is much thicker (610 nm) than V_2O_5 film. Different from pure V_2O_5 film, the cross section of the composite film with a V_2O_5/WO_3 molar ratio of 10:1 shows a granular structure, although the particles are smaller than pure WO_3 film. The thickness of this composite film is ~265 nm, thicker than V_2O_5 film but thinner than WO_3 film. Since the bulk density of WO_3 (7.25 g/cm^3) is much larger than that of V_2O_5 (3.35 g/cm^3) and all the films have the same mass, the WO_3 film with the largest thickness is the most porous and the V_2O_5 film with the lowest thickness is the least porous. The V_2O_5–WO_3 composite film with the intermediate thickness is more porous than V_2O_5 film and less porous than WO_3 film. Thus the composite film has larger electrochemical active area than V_2O_5 film, which can contribute to the enhanced Li-ion intercalation property of the composite film. However, the most porous WO_3 film delivers the lowest discharge capacity despite its porous structure and large surface area. It should be noted that the capacity of WO_3 is dependent on the potential range used in electrochemical measurements. For example, according to the work of Li and Fu [52], WO_3 exhibits a capacity of above 800 mA h/g in the potential range of 4.0–0.0 V vs. Li/Li$^+$, but the WO_3 sample exhibits much lower capacity when the potential range is reduced to 4.0–2.0 V vs. Li/Li$^+$. The potential range we used (0.4 to −1.6 V vs. Ag/Ag$^+$) is similar to the latter and thus our pure WO_3 film shows low capacity.

Fig. 5 shows typical cyclic voltammograms (CV) of V_2O_5, WO_3 and V_2O_5–WO_3 composite films heated at 470 °C measured at a scan rate of 0.05 V/s. The CV curve of WO_3 film shows indistinguishable cathodic and anodic peaks, indicating there is not much Li-ion intercalation/deintercalation within the given potential limit. On the other hand, the cyclic voltammogram of V_2O_5 film is more complicated. It shows two discernable cathodic peaks at −0.443 V, −0.735 V and three shoulders around −0.217 V, −1.179 V and −1.388 V; it shows three anodic peaks at −0.028 V, −0.547 V,−0.877 V and one shoulder around −0.240 V. The presence of cathodic and anodic peaks is attributed to Li$^+$ intercalation and extraction processes, respectively. The CV curve of the composite film with a V_2O_5/WO_3 molar ratios of 4:1 shows three cathodic peaks at −0.240 V, −0.438 V and −0.770 V and two shoulders around −1.148 V and −1.382 V; it shows anodic peaks at −0.071 V, −0.275 V, −0.560 V, −0.794 V and one shoulder around −1.201 V. This CV curve is similar to that of the pure V_2O_5 film. However, the shoulder around −0.217 V becomes a more discernable peak in the curve of this composite film with a V_2O_5/WO_3 molar ratio of 4:1, indicating enhanced kinetics for Li-ion intercalation in the composite film. For the film with a V_2O_5/WO_3 molar ratio of 1:1, two cathodic peaks are at −0.217 V and −0.421 V and three shoulders are around −0.706 V, −1.149 V and −1.370 V; three anodic peaks are at −0.170 V, −0.601 V and −0.794 V and two shoulders are around −0.304 V and −1.225 V. The positions of the cathodic peaks and shoulders are similar to those on the CV curve of pure V_2O_5, but the peaks are less discernable, indicating decreased kinetic property for Li-ion intercalation compared to the pure V_2O_5 film, which

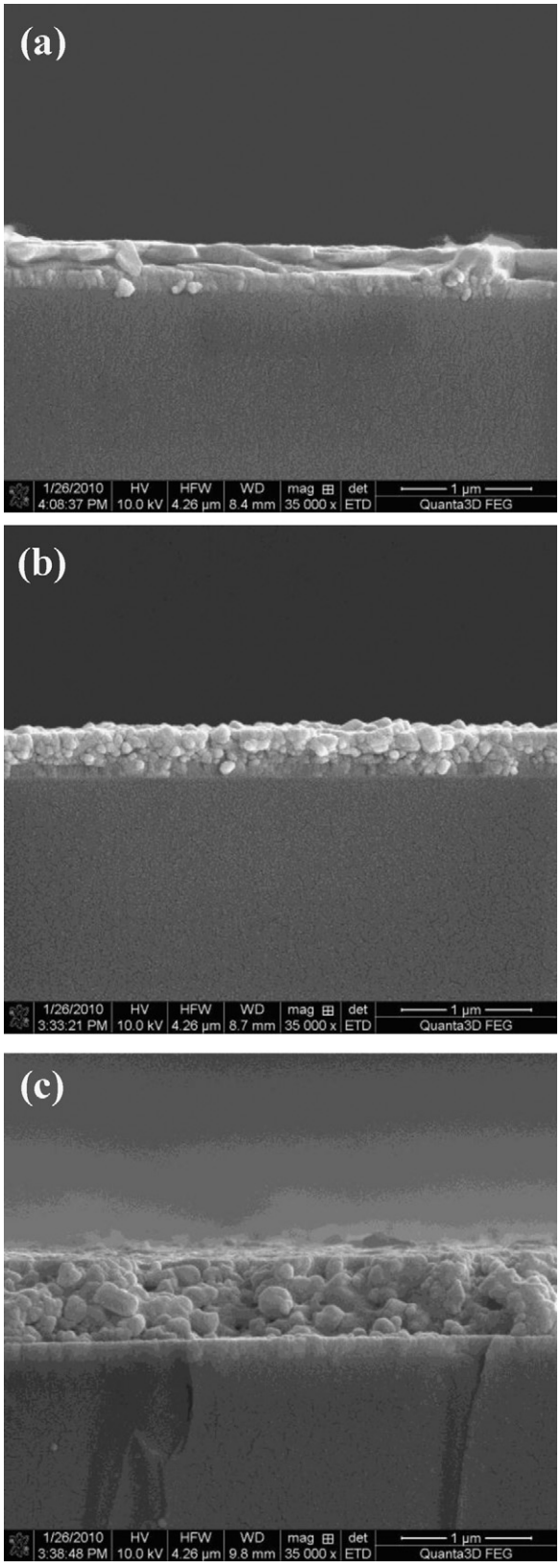

Fig. 4. SEM micrographs showing cross-section morphologies of (a) pure V_2O_5 film, (b) composite V_2O_5–WO_3 film with a V_2O_5:WO_3 molar ratio of 10:1, and (c) pure WO_3 film. All the films are obtained via annealing at 470 °C for 1 h.

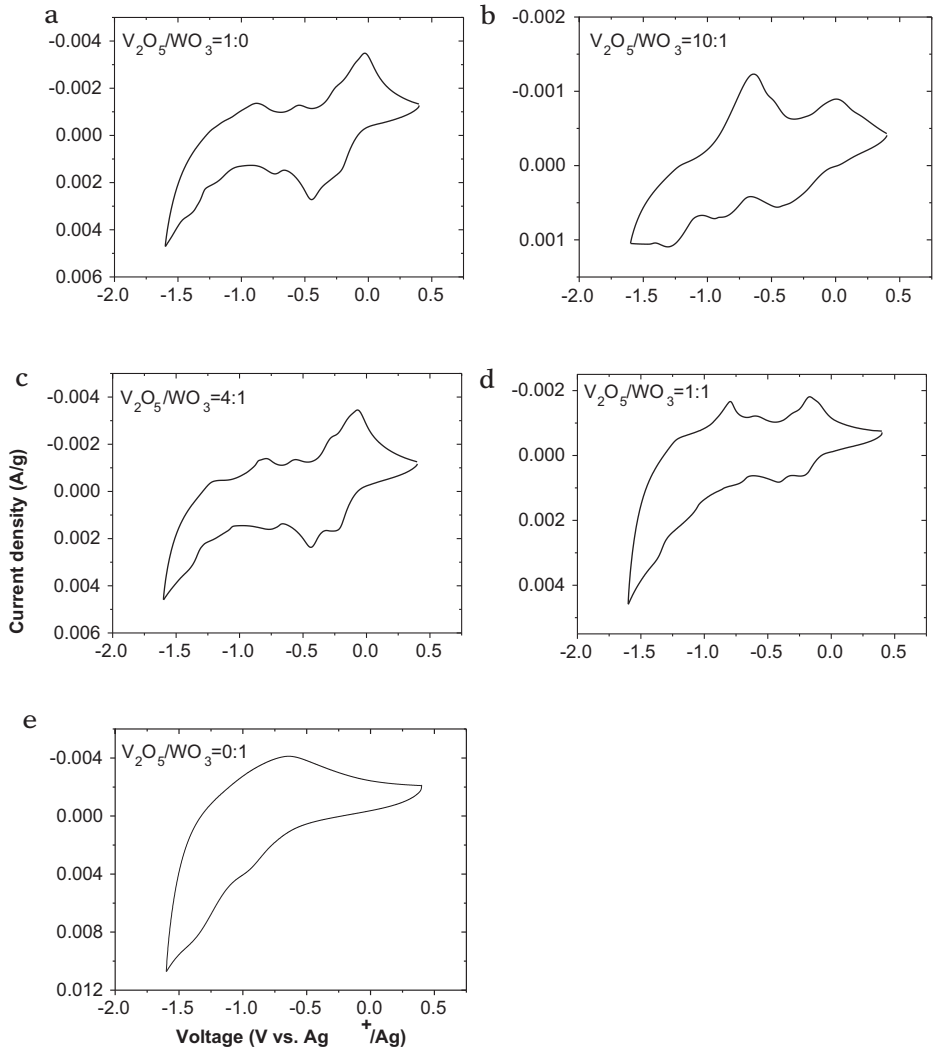

Fig. 5. Cyclic voltammograms of V_2O_5 film, WO_3 film, and composite V_2O_5–WO_3 films with V_2O_5/WO_3 = (a) 1:0, (b) 10:1, (c) 4:1, (d) 1:1 and (e) 0:1. The scan rate is 0.05 V/s.

can be ascribed to the increase of the amount of WO_3. On the other hand, the anodic peak at −0.170 V shifts to a more negative position and the peak at −0.794 V shifts to a more positive position compared to the peaks in the curve of pure V_2O_5 film. The curve obtained by the composite film (V_2O_5:WO_3 = 10:1) exhibits a simpler and considerably different profile compared to the CV curve of pure V_2O_5 film: both anodic and cathodic peaks shift appreciably; the cathodic peaks shift to −0.463 V, −0.949 V and −1.307 V, and the anodic peaks and shoulders shift to −0.008 V, −0.482 V and −0.642 V. Not only the position of the peaks and shoulders shift obviously, but also the shape of them change appreciably, which indicates that phase transitions during electrochemical intercalation/deintercalation in this composite film are different from those occurring in the pure V_2O_5 film. Similar results have also been observed from chronopotentiometric measurements as discussed below.

Fig. 6 illustrates the chronopotentiometric (CP) curves of the films heated at 470 °C with various V_2O_5/WO_3 molar ratios of 1:0, 10:1, 4:1, 1:1, 1:4 and 0:1 under a current density of 1.33 A/g. The CP curve of V_2O_5/WO_3 = 1:0 (pure V_2O_5) shows a stepwise shape with two plateaus starting at −0.43 V and −1.22 V, which are ascribed to two phase changes of $Li_xV_2O_5$ during Li^+ intercalation [19,53]. On the other hand, the CP curve of WO_3 film shows a sloping shape without stages. The CP curves of composite films with V_2O_5/WO_3 molar ratios of 4:1 and 10:1 also show two plateaus, similar to those of pure V_2O_5, but the plateaus in the CP curve of the composite film are less distinct, suggesting the deterioration of crystallinity of V_2O_5 caused by WO_3. Both of these two composite films show enhancement of Li-ion intercalation in the first phase change process.

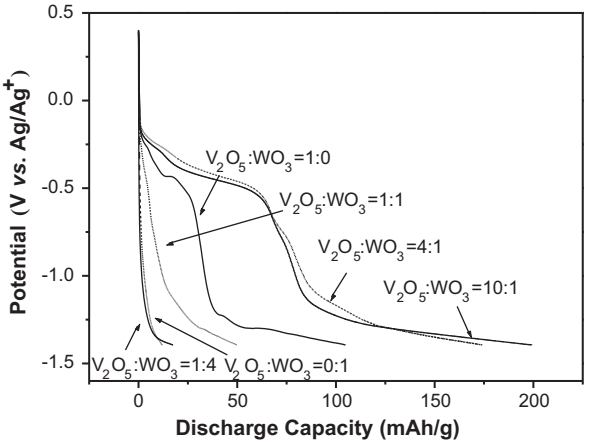

Fig. 6. Chronopotentiometric curves of V_2O_5 film, WO_3 film, and composite V_2O_5–WO_3 films with various V_2O_5/WO_3 molar ratios, at a constant current density of 1.33 A/g.

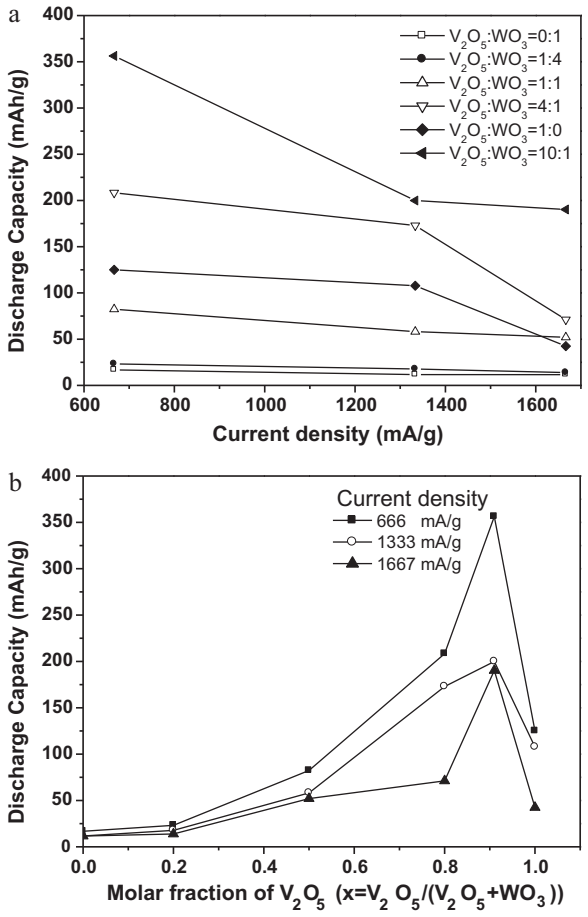

Fig. 7. (a) Summary of the discharge capacities of various V_2O_5–WO_3 composite films (a) as a function of current density, and (b) as a function of molar fractions of V_2O_5 (the moles of V_2O_5 divided by the total moles of V_2O_5 and WO_3).

However, the composite film with a molar ratio of V_2O_5/WO_3 = 10:1 delivers a higher capacity of 100 mA h/g in the potential range of −1.22 V and −1.4 V, whereas the pure V_2O_5 film and the composite film with a molar ratio of V_2O_5/WO_3 = 4:1 deliver a similar capacity of 65 mA h/g. The CP curves of composite films with V_2O_5/WO_3 molar ratios of 1:1 and 1:4 only have a gradual potential decrease without any distinct stepwise potential drop, similar to that of pure WO_3. Such disappearance of stepwise potential drop with increased WO_3 composition in the V_2O_5–WO_3 composite films further indicates the amorphization of V_2O_5 caused by addition of WO_3. As can be clearly seen from Fig. 6, the composite film with a V_2O_5/WO_3 molar ratio of 10:1 delivers the highest discharge capacity of 200 mA h/g than all other films at the same current density of 1.33 A/g, for example, almost twice of that delivered by pure V_2O_5 film (108 mA h/g). The coulombic efficiency of the composite film with a V_2O_5/WO_3 molar ratio of 10:1 is 70.5% which is slightly higher than that of the pure V_2O_5 film (67.5%).

Fig. 7a summarizes the discharge capacity as a function of current density for pure V_2O_5 and WO_3 films, and various composite V_2O_5–WO_3 films. When a relatively small amount of WO_3 is added into V_2O_5 as in the case of composite films with V_2O_5/WO_3 molar ratios of 4:1 and 10:1, the discharge capacity can be enhanced compared to pure V_2O_5 film. However, the Li^+ intercalation capacity is reduced compared to that of pure V_2O_5 film, when too much WO_3 is added into V_2O_5 as in the case of composite film with a V_2O_5/WO_3 molar ratio of 1:1. The discharge capacity of the composite film is greatly reduced when WO_3 is the major composition and plays a dominant role. Fig. 7b shows the change of discharge

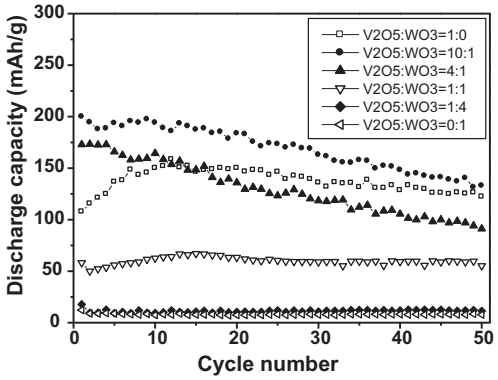

Fig. 8. Cycling performances of V_2O_5 film, WO_3 film, and composite V_2O_5–WO_3 films with various V_2O_5/WO_3 molar ratios, at a current density of 1.33 A/g.

capacity as a function of molar fraction of V_2O_5 (the moles of V_2O_5 divided by the total moles of V_2O_5 and WO_3) at different current densities. The discharge capacity first increases gradually with the increased amount of V_2O_5 in the composite films, but reaches the highest value with the V_2O_5/WO_3 molar ratio of 10:1 showing 356 mA h/g, 200 mA h/g and 190 mA h/g at current densities of 0.666 A/g, 1.333 A/g and 1.667 A/g, respectively. The trend of capacity vs. molar fraction is the same for all the three different current densities.

Fig. 8 compares the cycling performances of pure V_2O_5, pure WO_3 and the composite films with different V_2O_5/WO_3 molar ratios at a current density of 1.33 A/g. It can be seen that the composite film with a V_2O_5/WO_3 molar ratio of 10:1 delivers the highest capacity at every cycle compared to other samples. It shows the highest initial discharge capacity of 200 mA h/g, and maintains a highest capacity of 132 mA h/g after 50 cycles. The cycling performance of pure V_2O_5 shows an increasing trend in initial cycles followed by degradation. The initial discharge capacity of pure V_2O_5 film is not high, but there is an increase of the discharge capacity between the 2nd cycle and the 13th cycle. Similar phenomena have been reported in literature [16]. The increase in initial capacities of V_2O_5 film can be attributed to the deterioration of crystallinity of V_2O_5 during initial cycling [16]. For the composite film with a V_2O_5/WO_3 molar ratio of 4:1, the initial capacity is higher than that of pure V_2O_5 film but lower than that of the composite film with a V_2O_5/WO_3 molar ratio of 10:1. However, this composite film with a molar ratio of 4:1 shows poor cycling performance. The capacity decreases to 91 mA h/g after 50 cycles, which is even lower than that of pure V_2O_5 film (122 mA h/g). When the molar ratio of WO_3 increases gradually, the capacities delivered by the composite films (V_2O_5:WO_3 = 1:1, 1:4, 0:1) decrease considerably, although the capacity retention is relatively stable. These results are due to the poor electrochemical activity of WO_3 in this potential range as discussed earlier.

The enhanced electrochemical properties of composite films can be attributed to the reduced grain size as shown in the XRD patterns (Fig. 1) and the increased porosity as shown in the SEM images (Figs. 3 and 4). Therefore, the composite film with smaller grain size provides larger electrochemical active surface area and shorter diffusion length for the Li-ion intercalation process. The composite films show an amorphous or partially amorphous phase from the XRD patterns in Fig. 1, which facilitates the intercalation of Li ions [54].

4. Conclusions

V_2O_5–WO_3 composite films with enhanced intercalation properties have been prepared by a solution method without

introducing any impurity elements. XRD, SEM and electrochemical measurements have been employed to reveal the structure and properties of these films. XRD analysis indicates that the addition of WO_3 greatly reduces the crystallinity of V_2O_5, which results in enhanced Li-ion insertion capacities. SEM images show that fibers with different diameters are dispersed in porous films in the composite films, leading to higher surface area. Both the CV and CP curves of the V_2O_5–WO_3 film with the molar ratio of 10:1 are distinctively different from those of V_2O_5 film, suggesting a different Li-ion intercalation process in the V_2O_5–WO_3 film with the molar ratio of 10:1. The V_2O_5–WO_3 film with the molar ratio of 10:1 delivers the highest discharge capacities of 200 mA h/g at the first cycle and 132 mA h/g after 50 cycles at a current density of 1.33 A/g, compared to pure oxide films and other composite films with different molar ratios; for example, the pure V_2O_5 film delivers only 108 mA h/g at the first cycle at the same current density. The enhanced Li-ion intercalation properties of V_2O_5–WO_3 composite films are attributed to both morphological and structural changes in one oxide induced by the presence of other oxide.

Acknowledgments

The work is financially supported by the LSU junior faculty start-up funds. C. Cai and D.S. Guan would like to acknowledge the LSU Graduate School Enhancement Award and Graduate School Supplementary Award, respectively. The authors also thank Materials Characterization Center at LSU for technical support in using XRD and SEM.

References

[1] B. Kang, G. Ceder, Nature 458 (2009) 190–193.
[2] W. Wu, Y. Wang, X.Y. Wang, Q.Q. Chen, X. Wang, S.Y. Yang, X.M. Liu, J. Guo, Z.H. Yang, J. Alloys Compd. 486 (2009) 93–96.
[3] Y.-C. Si, L.-F. Jiao, H.-T. Yuan, H.-X. Li, Y.-M. Wang, J. Alloys Compd. 486 (2009) 400–405.
[4] A.Y. Shenouda, H.K. Liu, J. Alloys Compd. 477 (2009) 498–503.
[5] S.B. Tang, M.O. Lai, L. Lu, J. Alloys Compd. 449 (2008) 300–303.
[6] F. Teng, S. Santhanagopalan, Y. Wang, D.D. Meng, J. Alloys Compd. 499 (2010) 259–264.
[7] W. Huang, S.K. Gao, X.K. Ding, L.L. Jiang, M.D. Wei, J. Alloys Compd. 495 (2010) 185–188.
[8] Q.T. Qu, Y. Shi, L.L. Li, W.L. Guo, Y.P. Wu, H.P. Zhang, S.Y. Guan, R. Holze, Electrochem. Commun. 11 (2009) 1325–1328.
[9] W.-C. Fang, J. Phys. Chem. C 112 (2008) 11552–11555.
[10] C.G. Granqvist, Handbook of Inorganic Electrochromic Materials, Elsevier, Amsterdam, 1995.
[11] N.A. Galiote, F. Huguenin, J. Phys. Chem. C 111 (2007) 14911–14916.
[12] A. Wolcott, T.R. Kuykendall, W. Chen, S. Chen, J.Z. Zhang, Phys. Chem. B 110 (2006) 25288–25296.
[13] M.S. Whittingham, Chem. Rev. 104 (2004) 4271–4302.
[14] C. Navone, J.P. Pereira-Ramos, R. Baddour-Hadjean, R. Salot, J. Power Sources 146 (2005) 327–330.
[15] Y. Wang, G.Z. Cao, Adv. Mater. 20 (2008) 2251–2269.
[16] D. Liu, Y.Y. Liu, B.B. Garcia, Q.F. Zhang, A.Q. Pan, Y.-H. Jeong, G.Z. Cao, J. Mater. Chem. 19 (2009) 8789–8795.
[17] A.Q. Pan, D.W. Liu, X.Y. Zhou, B.B. Garcia, S.Q. Liang, J. Liu, G.Z. Cao, J. Power Sources 195 (2010) 3893–3899.
[18] M.S. Whittingham, J. Electrochem. Soc. 123 (1976) 315–320.
[19] F. Lantelme, A. Mantoux, H. Groult, D.J. Lincot, J. Electrochem. Soc. 150 (2003) A1202–A1208.
[20] K. Lee, G.Z. Cao, J. Phys. Chem. B 109 (2005) 11880–11885.
[21] K.E. Swider-Lyons, C.T. Love, D.R. Rolison, Solid State Ionics 152–153 (2002) 99–104.
[22] V.M. Mohan, B. Hu, W.L. Qiu, W. Chen, J. Appl. Electrochem. 39 (2009) 2001–2006.
[23] C.R. Xiong, A.E. Aliev, B. Gnade, K.J. Balkus Jr., ACS Nano 2 (2008) 293–301.
[24] A.P. Jin, W. Chen, Q.Y. Zhu, Y. Yang, V.L. Volkov, G.S. Zakharova, Thin Solid Films 517 (2009) 2023–2028.
[25] T. Watanabe, Y. Ikeda, T. Ono, M. Hibino, M. Hosoda, K. Sakai, T. Kudo, Solid State Ionics 151 (2002) 313–320.
[26] F. Coustier, J. Hill, B.B. Owens, S. Passerini, W.H.J. Smyrl, Electrochem. Soc. 146 (1999) 1355–1360.
[27] Livage, J. Chem. Mater. 3 (1991) 578–593.
[28] Y. Dimitriev, V. Dimitrov, M. Arnaudov, D.J. Topalov, Non-Cryst. Solids 57 (1983) 147–156.
[29] N. Machida, R. Fuchida, T.J. Minami, Electrochem. Soc. 136 (1989) 2133–2136.
[30] S.Y. Zhan, C.Z. Wang, K. Nikolowski, H. Ehrenberg, G. Chen, Y.J. Wei, Solid State Ionics 180 (2009) 1198–1203.
[31] M.J. Parent, S. Passerini, B.B. Owens, W.H.J. Smyrl, Electrochem. Soc. 146 (1999) 1346–1350.
[32] T. Kudo, Y. Ikeda, T. Watanabe, M. Hibino, M. Miyayama, H. Abe, K. Kajita, Solid State Ionics 152–153 (2002) 833–841.
[33] D. Zhu, H. Liu, L. Lv, Y.D. Yao, W.Z. Yang, Scripta Mater. 59 (2008) 642–645.
[34] K. Takahashi, Y. Wang, K. Lee, G. Cao, Appl. Phys. A 82 (2006) 27–31.
[35] M. Deepa, D.P. Singh, S.M. Shivaprasad, S.A. Agnihotry, Curr. Appl. Phys. 7 (2007) 220–229.
[36] C.G. Granqvist, Sol. Energy Mater. Sol. Cells 60 (2000) 201–211.
[37] J.M. Wang, E. Khoo, P.S. Lee, J. Ma, J. Phys. Chem. C 112 (2008) 14306–14312.
[38] S.K. Deb, Sol. Energy Mater. Sol. Cells 92 (2008) 245–258.
[39] N. Ozer, C.M. Lampert, Thin Solid Films 349 (1999) 205–211.
[40] D.-W. Kim, H. Kim, Y.-S. Jung, I.K. Song, S.-H. Baeck, J. Phys. Chem. Solids 69 (2008) 1513–1517.
[41] M. Najbar, F. Mizukami, P. Kornelak, A. Wesełucha-Birczyĭnska, B. Borzęcka-Prokop, E. Bielaĭnska, A. Białas, J. Banaĭs, D. Su, Catal. Today 90 (2004) 93–102.
[42] M. Ranjbar, S.M. Mahdavi, A. Iraji zad, Sol. Energy Mater. Sol. Cells 92 (2008) 878–883.
[43] G.J. Fang, K.-L. Yao, Z.-L. Liu, Thin Solid Films 394 (2001) 64–71.
[44] G.N. Barbosa, A.T. Bolsoni, H.P. Oliveira, J. Non-Cryst. Solids 354 (2008) 3548–3553.
[45] C.J. Fontenot, J.W. Wiench, M. Pruski, G.L.J. Schrader, Phys. Chem. B 104 (2000) 11622–11631.
[46] B. Yebka, B. Pecquenard, C. Julien, J. Livage, Solid State Ionics 104 (1997) 169–175.
[47] E.I. Rogers, D.S. Silvester, S.E.W. Jones, L. Aldous, C. Hardacre, A.J. Russell, S.G. Davies, R.G. Compton, J. Phys. Chem. C 111 (2007) 13957–13966.
[48] E. Abitelli, S. Ferrari, E. Quartarone, P. Mustarelli, A. Magistris, M. Fagnoni, A. Albini, C. Gerbaldi, Electrochim. Acta 55 (2010) 5478–5484.
[49] G.J. Fang, Z.L. Liu, Y.Q. Wang, H.H. Liu, K.L.J. Yao, Phys. D: Appl. Phys. 33 (2000) 3018–3021.
[50] M. Yagia, S. Maruyamaa, K. Sonea, K. Nagaib, T. Norimatsu, J. Solid State Chem. 181 (2008) 175–182.
[51] X.L. Sun, H.T. Cao, Z.M. Liu, J.Z. Li, Appl. Surf. Sci. 255 (2009) 8629–8633.
[52] W.-J. Li, Z.-W. Fu, Appl. Surf. Sci. 256 (2010) 2447–2452.
[53] C.J. Patrissi, C.R.J. Martin, Electrochem. Soc. 146 (1999) 3176–3180.
[54] F. Coustier, S. Passerini, W.H. Smyrl, Solid State Ionics 100 (1997) 247–258.